Electronic Supplementary Information

In-situ studies on controlling atomically-accurate formation process of gold nanoclusters

Lina Yang,[1†] Hao Cheng,[1†] Yong Jiang,[1] Ting Huang,[1] Jie Bao,[1] Zhihu Sun,[1*] Zheng Jiang,[2] Jingyuan Ma,[2] Fanfei Sun,[2] Qinghua Liu,[1] Tao Yao,[1*] Huijuan Deng,[3] Shuxin Wang,[3] Manzhou Zhu,[3] and Shiqiang Wei[1*]

[1]*National Synchrotron Radiation Laboratory, University of Science and Technology of China, Hefei 230029, P. R. China*
[2]*Shanghai Synchrotron Radiation Facility, Shanghai Institute of Applied Physics, Chinese Academy of Sciences, Shanghai 201204, P. R. China*
[3]*Department of Chemistry, Anhui University, Hefei 230039, P. R. China*

I. Characterization of the end product of nanoclusters

The synthesis of monodisperse $Au_{13}(L_3)_4Cl_4$ nanoclusters follows the protocol by Shichibu *et al*.,[1] involving two primary stage as schematically shown in Figure S1(a) and depicted in the main text. Figure S1(b) shows the transmission electron microscopy (TEM) image of the end product, indicating the attainment of monodisperse clusters with mean size of 1.1±0.1 nm. The UV-vis absorption spectrum of the obtained nanoclusters as displayed in Fig. S1(c) shows pronounced absorption peaked at 340 nm and a shoulder at 420 nm, in excellent agreement with those for $Au_{13}(L_3)_4Cl_4$ nanoclusters reported by Shichibu *et al*..[1] The distinct optical absorption and the absence of the 530 nm peak characteristic of Au nanocrystals (>2 nm) imply high purity and high yield of the as-synthesized nanoclusters subjected to no purification procedure, in good agreement with the TEM measurement. MALDI mass spectrometry was also employed to further characterize the size and identify the component of the end product. A series of MALDI-MS measurements using DCTB as the MALDI matrix at various laser pulse intensities were attempted as shown in Fig. S1(d). While high laser pulse intensities (relative intensity >30%) produced many peaks below m/z=4351 Da, at the low (20%) laser pulse intensity, a nearly single peak at m/z = 4351 Da could be readily observed and assigned to the intact $Au_{13}(L_3)_4Cl_4$ (m/z =4352.2 Da), in good agreement with the ESI-MS

† These authors contributed equally to this work.
* Corresponding authors. E-mail: zhsun@ustc.edu.cn; yaot@ustc.edu.cn; sqwei@ustc.edu.cn.

measurement by Shichibu *et al*..[1] This shows that using DCTB as the MALDI matrix and keeping the low enough laser pulse intensity could minimize the fragmentation and loss of ligands upon ionization. Summarizing these results, we conclude that monodispersive $Au_{13}(L_3)_4Cl_4$ nanolcusters have been obtained.

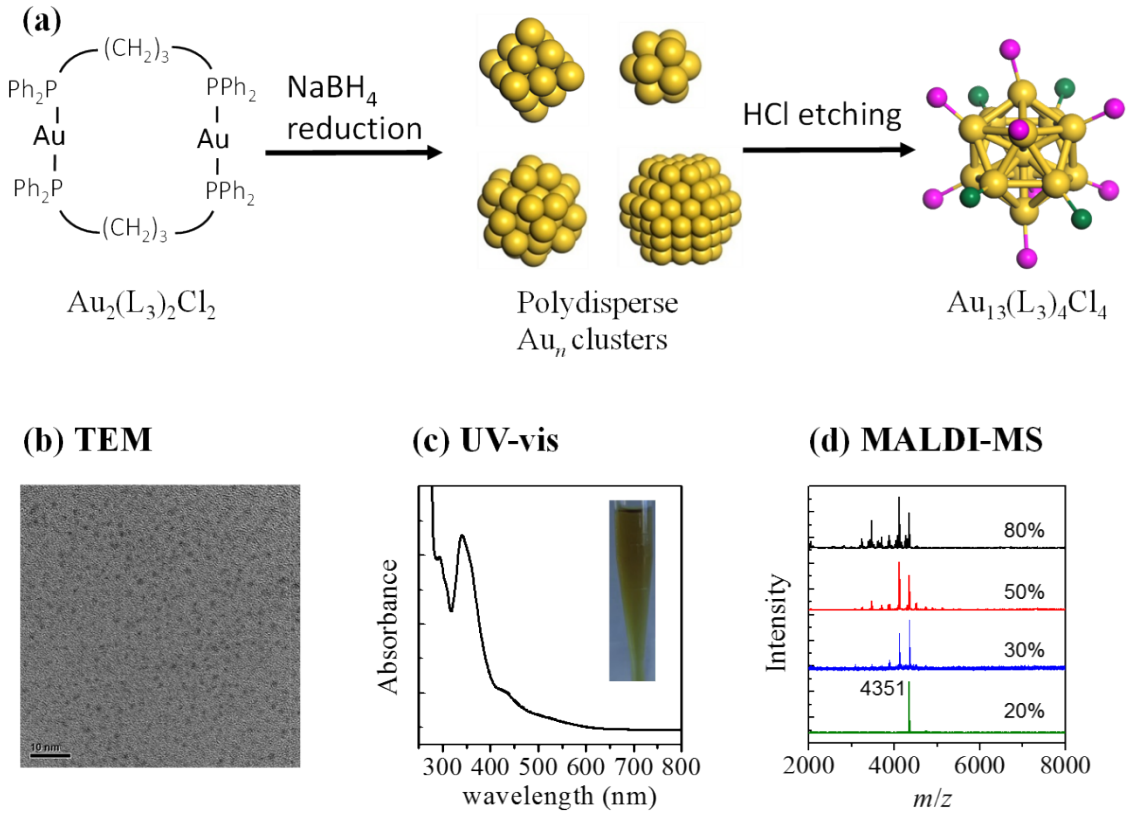

Figure S1. (a) Synthetic scheme, (b) TEM images, (c) UV-vis absorption spectrum and (d) MALDI mass spectrometry of the as-obtained Au clusters at various laser pulse intensities as leableed by the percentage numbers.

II. Characterization of the polydisperse L_3-protected Au_n precursor clusters

The precursor for forming $Au_{13}(L_3)_4Cl_4$ is polydisperse L_3-protected Au_n clusters, which were synthesized by reduction of $Au_2(L_3)Cl_2$ with $NaBH_4$ in dichloromethane solvent. Figure S2(a) shows the TEM image of the L_3-protected Au_n clusters, indicating the polydisperse nature with wide a size distribution. The UV-vis absorption spectrum in Fig. 2(b) demonstrates a wide hump at around 500 nm and no other fine structure. The MALDI mass spectrometry displayed in Fig. 2(c) covers a wide size range of 3000–13000 Da, corresponding to a rough mixture of Au_{15}–Au_{65} clusters.

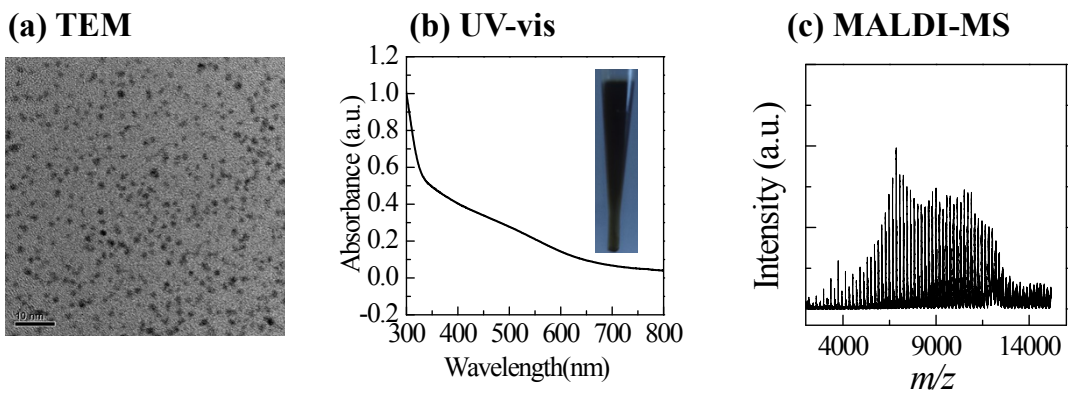

Figure S2. (a) TEM images, (b) UV-vis absorption spectrum and (c) MALDI mass spectrometry of the polydisperse L_3-protected Au_n clusters.

III. Assignment of the MALDI-MS peaks for Au_n clusters at 1 h reaction time

The MALDI mass spectrometry for the clusters at ~1 h of reaction is shown in Fig. S3. It shows that distinct MS peaks are located in two regions of roughly 6000–8000 and 3000–4000 Da. In the 6000–8000 Da size range, the spacing between neighboring main peaks is ~197 Da, suggesting a mixture of relatively large Au clusters ranging from ~Au_{30} to ~Au_{40}. According to Zhang et al[2], the apex sites of these clusters might be weakly ligated by the bulky L_3 ligands, while leaving the surface sites uncovered and active. The distinct peaks in the mass range of 3000–4000 Da are located at 3241, 3472, 3654, 3886, 4119, and 4351 Da, and the distances between the adjacent peaks are mostly ~232 Da corresponding to a AuCl (*m*/*z* =232.4 Da) unit. The dominant peak at 3886 Da is assigned to the composition of $Au_{11}(L_3)_4Cl_2$, and the other peaks could be assigned to: $Au_{13}(L_3)_4Cl_4$ (4351 Da), $Au_{12}(L_3)_4Cl_3$ (4119 Da), $Au_{10}(L_3)_4Cl$ (3654 Da), $Au_9(L_3)_4Cl$ (3472 Da), and $Au_8(L_3)_4$ (3241 Da).

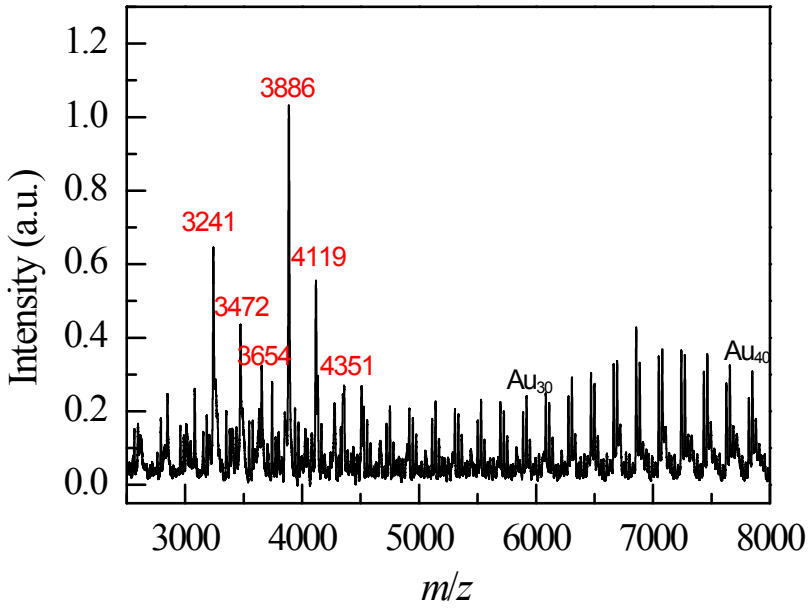

Figure S3. Zoom-in plot of the MALDI mass spectrometry of Au_n clusters at a reaction time of 1 h.

IV. EXAFS data analysis

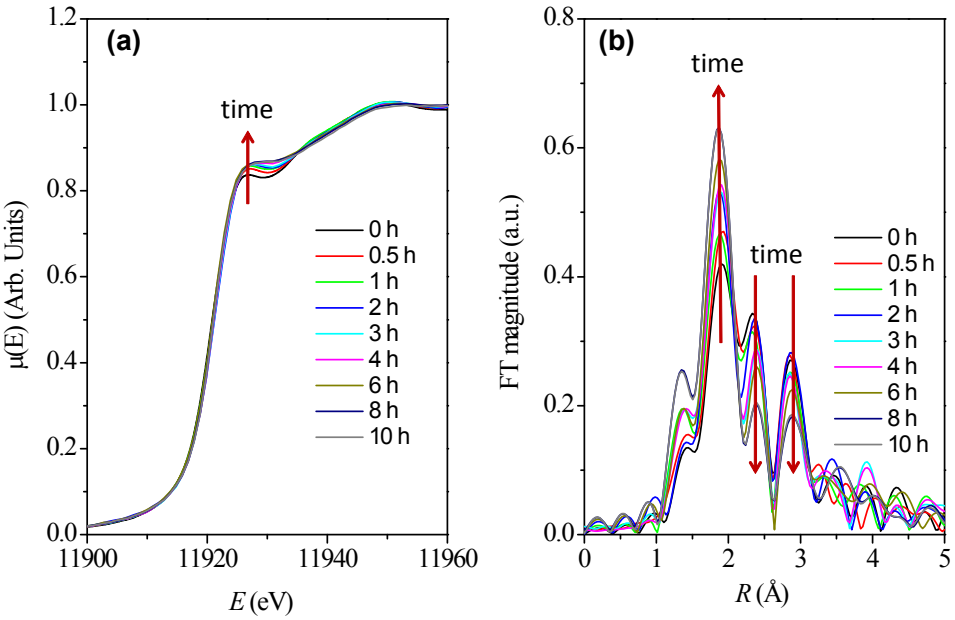

Figure S4. The time-dependent Au L_3-edge (a) XANES, (b) EXAFS spectra, same as those shown in Fig. 3 (a) and (b) in the main text but not shifted vertically.

The acquired EXAFS data were processed according to the standard procedures using the ATHENA module implemented in the IFEFFIT software packages,[3] and Figure S5(a) shows the obtained $\chi(k)$ oscillatory curves at different reaction time. The quantitative curve-fittings were carried out for the Fourier transformed k^2-weighted $\chi(k)$ in the R-space

with a Fourier transform k-space range of 3.0–12.0 Å^{-1} using the module ARTEMIS[4] of IFEFFIT. The backscattering amplitude $F(k)$ and phase shift $\Phi(k)$ were calculated using FEFF8.0 code.[5] During the curve-fitting, the overall amplitude reduction factor S_0^2 was fixed to the best-fit value of 0.90 determined from fitting the data of Au foil. Because EXAFS is incapable of distinguishing P from Cl neighbors, we treated them cumulatively as Au-ligand pairs.[6-8] To fit the data in the R-range of 1.4–3.6 Å, we considered an Au−ligand and two Au–Au pairs standing for the central-peripheral and peripheral-peripheral Au–Au bonds in an incomplete or complete icosahedron (labelled as Au–Au (c-p) and Au–Au (p-p), respectively). For each pair, the structural parameters, such as the coordination number N, interatomic distance R, and the Debye–Waller factor σ^2 were allowed to vary. For the two Au–Au pairs, common adjustable parameters of edge-energy shift ΔE_0 and σ^2 were used to reduce the number of free parameters. In addition, we included a variable of third-order cumulant C^3 for the Au–Au pairs to account for the inharmonic pair distribution function. The obtained structural parameters are summarized in Table S1 and plotted in Figures 3(c)-(e) in the main text. The curve-fitting results at different reaction times are shown in Figure S5(b).

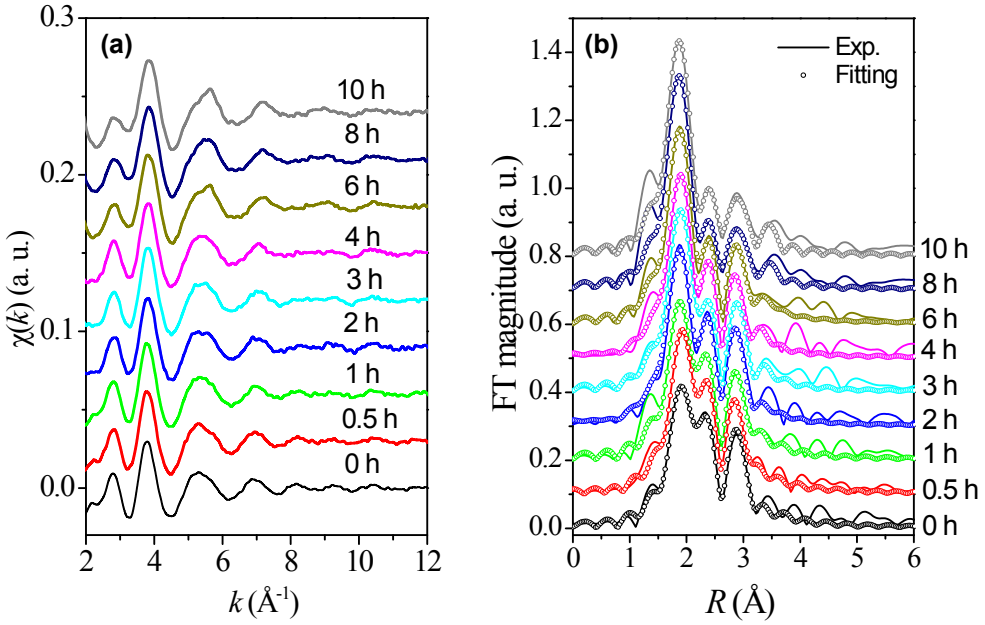

Figure S5. (a) The EXAFS $\chi(k)$ oscillatory curves, and (b) R-space EXAFS curve-fitting results for the Fourier transformed k^2-weighted $\chi(k)$ functions at different times of reaction. The solid lines and circles donate the experimental data and the fitting results, respectively.

Table S1. Structural parameters of Au nanoclusters extracted from least-squares curve-fitting of the EXAFS spectra at different HCl-etching reaction time.

Reaction time	Bond	*N*	*R* (Å)	σ^2 (10^{-3}Å^2)	ΔE (eV)
0 h	Au-P/Cl	0.58±0.04	2.31±0.01	3.1±0.3	3.2±0.5
	Au-Au (c-p)	6.8±1.1	2.83±0.04	14.0±1.4	4.0±1.1
	Au-Au (p-p)	2.8±1.2	3.08±0.06	14.0±1.4	4.1±0.9
0.5 h	Au-P/Cl	0.75±0.05	2.33±0.01	3.0±0.3	3.2±0.6
	Au-Au (c-p)	6.6±1.1	2.84±0.04	14.0±1.4	3.8±1.1
	Au-Au (p-p)	2.5±1.2	3.10±0.06	14.0±1.4	4.4±0.8
1 h	Au-P/Cl	0.80±0.09	2.31±0.01	2.9±0.3	3.2±0.6
	Au-Au (c-p)	6.5±1.1	2.84±0.04	13.9±1.5	3.8±1.1
	Au-Au (p-p)	2.7±1.1	3.07±0.06	13.9±1.5	4.4±0.8
2 h	Au-P/Cl	0.91±0.13	2.28±0.01	3.1±0.3	3.6±0.6
	Au-Au (c-p)	6.2±1.1	2.80±0.04	13.5±1.4	3.8±1.0
	Au-Au (p-p)	2.8±1.4	3.06±0.06	13.5±1.4	4.2±0.7
3 h	Au-P/Cl	0.98±0.11	2.30±0.01	3.1±0.3	3.2±0.6
	Au-Au (c-p)	5.6±0.8	2.77±0.05	13.8±1.4	3.8±1.1
	Au-Au (p-p)	3.3±1.0	3.02±0.06	13.8±1.4	4.4±0.8
4 h	Au-P/Cl	1.07±0.12	2.30±0.01	2.8±0.3	3.2±0.5
	Au-Au (c-p)	4.5±0.9	2.79±0.06	14.2±1.4	3.9±0.9
	Au-Au (p-p)	3.4±1.0	3.03±0.06	14.2±1.4	4.1±0.6
6 h	Au-P/Cl	1.21±0.12	2.28±0.01	2.9±0.3	3.2±0.4
	Au-Au (c-p)	3.8±0.8	2.76±0.06	14.7±1.5	4.1±1.1
	Au-Au (p-p)	3.6±0.6	2.97±0.07	14.7±1.5	4.3±0.7
8 h	Au-P/Cl	1.22±0.12	2.28±0.01	3.0±0.3	3.2±0.6
	Au-Au (c-p)	3.5±0.8	2.71±0.06	14.4±1.5	3.8±1.1
	Au-Au (p-p)	3.5±0.8	2.95±0.08	14.4±1.5	4.4±0.8
10 h	Au-P/Cl	1.21±0.12	2.28±0.013	3.0±0.3	3.2±0.4
	Au-Au (c-p)	3.3±0.8	2.72±0.06	14.9±1.5	4.1±1.1
	Au-Au (p-p)	3.4±0.8	2.94±0.08	14.9±1.5	4.3±0.7

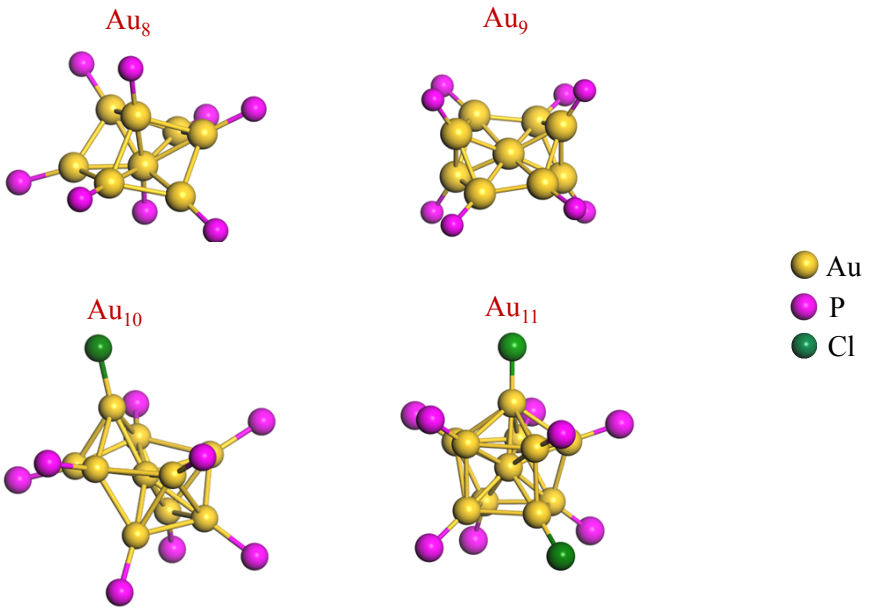

Figure S6. Schematic structures of the possible Au_8–Au_{11} intermediate clusters during the formation of Au_{13} clusters. For clarity, two phenyl rings and a C_3H_6 chain connected to every P atom are omitted.

V. Experiments using sulfuric acid and acetic acid as etchants

Independent experiments replacing HCl with sulfuric acid (H_2SO_4, 68 μL, 98%) or acetic acid (CH_3COOH, 200 μL, >98%) under the otherwise identical conditions were also attempted. UV-vis absorption spectra were employed to monitor the reactions and the results are shown in Fig. S7 (a) and (b), respectively. After 3 h of H_2SO_4 treatment, the 420 nm absorption peak indicates the formation of smaller clusters, like what we observe in the HCl case. In the case of CH_3COOH treatment, the spectral change is much slower. We monitored the time course of CH_3COOH treatment by *in-situ* XAFS measurement. The Fourier transformed EXAFS spectra Fig. S8 indicate that the Au-Au peak is obviously decreased in intensity with increasing reaction time. These experiments add more support to the H^+-induced decomposition of the larger Au_n mixture.

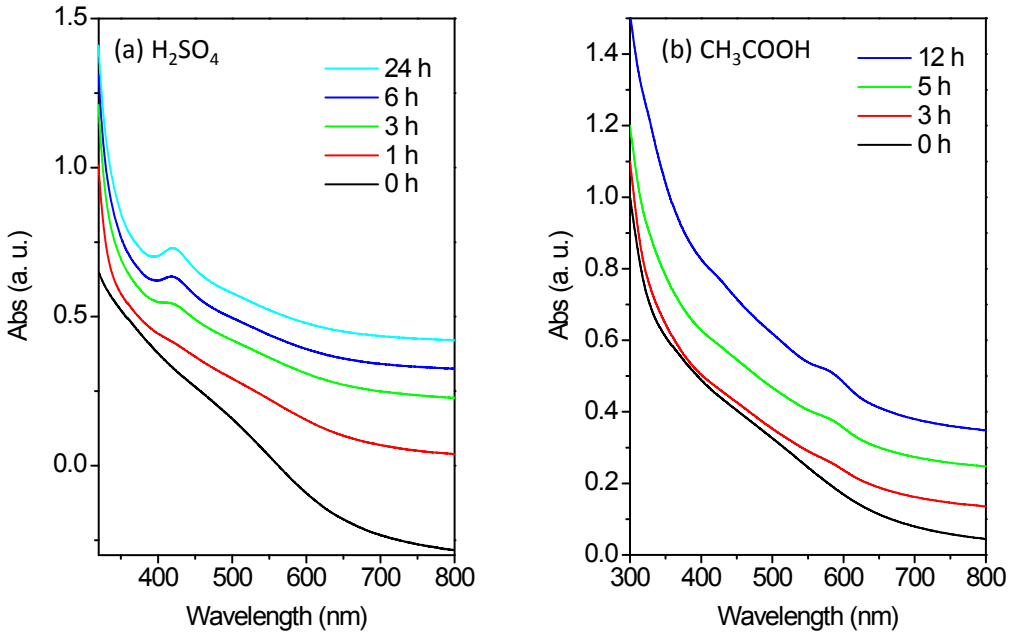

Figure S7. Time-dependent UV-vis absorption spectra of the etching course by using (a) H_2SO_4, and (b) CH_3COOH as the etchants.

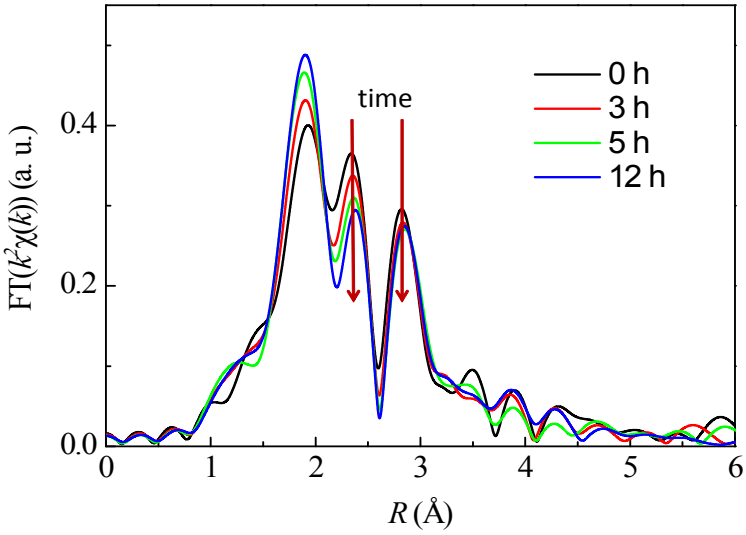

Figure S8. Time-dependent Fourier transformed EXAFS spectra of the etching course by using CH_3COOH as the etchant.

VI. Growth from Au_{11} to Au_{13} in HCl environment

A parallel experiment is designed to grow isolated Au_{11} into Au_{13} clusters, through reaction of Au_{11} with HCl and $AuClPPh_3$ that provides the Au(I)-Cl oligomers. The Au_{11} clusters were synthesized using a conventional method.[9-12] Typically, $AuClPPh_3$ (10 mg) was dissolved in deaerated $CHCl_3$ (20 ml) under stirring and Ar. To the solution 8 mg L_3 was added and then 8.7 mg boranetert-butylamine (TBAB) was added to reduce the mixture for 3 h. The MALDI mass spectrum in Fig. 4(a) of the main text was employed to identify the product. The peak at around *m/z*=3885 Da indicates the successful

synthesis of $Au_{11}(L_3)_4Cl_2$. Then, $AuClPPh_3$ (4 mg, 8 μmol) and HCl (150 μl, 1.4 mmol) were added to an ethanol solution (5 ml) of $Au_{11}(L_3)_4Cl_2$ (5.6 mg, 1.5 μmol) successively and the mixture was stirred at room temperature. After 7 h, the end product was obtained. The MALDI mass spectrum displays a peak at *m/z*= 4351 Da (Figure 5(b)), corresponding to $Au_{13}(L_3)_4Cl_4$. The time-dependent UV-vis absorption spectra measurements were performed to monitor the HCl-induced growth process from Au_{11} to Au_{13}, and the results are displayed in Fig. 4(b) of the main text.

References

1. Y. Shichibu, K. Suzuki and K. Konishi, *Nanoscale*, 2012, **4**, 4125-4129.
2. H. F. Zhang, M. Stender, R. Zhang, C. M. Wang, J. Li and L. S. Wang, *J. Phys. Chem. B*, 2004, **108**, 12259-12263.
3. M. Newville, *J. Synchrotron Rad.*, 2001, **8**, 322-324.
4. B. Ravel and M. Newville, *J. Synchrotron Rad.*, 2005, **12**, 537-541.
5. A. L. Ankudinov, B. Ravel, J. J. Rehr and S. D. Conradson, *Phys. Rev. B*, 1998, **58**, 7565-7576.
6. Y. Jiang, P. D. Yin, Y. Y. Li, Z. H. Sun, Q. H. Liu, T. Yao, H. Cheng, F. C. Hu, Z. Xie, B. He, G. Q. Pan and S. Q. Wei, *J. Phys. Chem. C*, 2012, **116**, 24999-25003.
7. Y. Y. Li, H. Cheng, T. Yao, Z. H. Sun, W. S. Yan, Y. Jiang, Y. Xie, Y. F. Sun, Y. Y. Huang, S. J. Liu, J. Zhang, Y. N. Xie, T. D. Hu, L. N. Yang, Z. Y. Wu and S. Q. Wei, *J. Am. Chem. Soc.*, 2012, **134**, 17997-18003.
8. Y. Jiang, Y. Y. Huang, H. Cheng, Q. H. Liu, Z. Xie, T. Yao, Z. Jiang, Y. Y. Huang, Q. Bian, G. Q. Pan, Z. H. Sun and S. Q. Wei, *J. Phys. Chem. C*, 2014, **118**, 714-719.
9. Y. Kamei, Y. Shichibu and K. Konishi, *Angew. Chem. Int. Ed.*, 2011, **50**, 7442-7445.
10. M. F. Bertino, Z. M. Sun, R. Zhang and L. S. Wang, *J. Phys. Chem. B*, 2006, **110**, 21416-21418.
11. J. M. M. Smits, J. J. Bour, F. A. Vollenbroek and P. T. Beurskens, *Journal of Crystallographic and Spectroscopic Research*, 1983, **13**, 355-363.
12. K. P. Hall and D. M. P. Mingos, *Prog. Inorg. Chem.*, 1984, **32**, 237-325.